PROGRESS REPORT

High-Spatial-Resolution Passive Microwave Sounding Systems

NASA Grant NAG 5-10

covering the period
August 1, 1989 - January 31, 1990

Submitted by

D. H. Staelin
J. W. Barrett
P. G. Bonanni
W. J. Chiarchiaro II
P. W. Rosenkranz

July 26, 1990

Massachusetts Institute of Technology
Research Laboratory of Electronics
Cambridge, Massachusetts 02139

High-Spatial-Resolution

Passive Microwave Sounding Systems

During this period the emphasis was on: 1) improvement of the 54-GHz portion of the 54-118 GHz microwave temperature sounder (MTS) aircraft radiometer system in preparation for future observations, 2) related theoretical work predicting to what degree upper stratospheric temperatures will be observable from the ground using the new high-spectral resolution capabilities of the MTS, and 3) continued development of procedures for detecting and analyzing thermal waves in our 118-GHz MTS imagery. Support continued for publication of the results from earlier high-spatial-resolution passive microwave observations from aircraft near 118 GHz and 53.6 GHz.

1. RECEIVER IMPROVEMENTS

These improvements were motivated by the near demise of the present MTS 53-GHz radiometer, originally developed in the early 1970s and used for our most recent experiments on the NASA ER-2 aircraft.. Many elements are being replaced, and since the state of the art has advanced considerably in these 15 years, the new system will also be far more capable.

The design of the RF and video signal paths was completed for the new 54-GHz radiometer, from the calibration switch to the wideband detector and autocorrelator. Two versions of a phase-locking subsystem for the Watkins-Johnson 54-GHz Gunn local oscillator were also designed. The Watkins-Johnson 54-GHz first mixer (with integral IF amplifier) will be followed by an Avantek UTO-558 modular amplifier which will drive a cascade of a 30-MHz highpass filter and a 200-MHz lowpass filter. These filters, made by K & L, will define a passband which will emulate that of a typical AMSU-A channel. Another UTO-558 amplifier and a 3-dB splitter will follow. One output of the splitter will be further amplified by a UTO-558 and finally passed to a square-law detector. This will be the wideband, or AMSU-A, channel.

The other output of the splitter will go through a UTO-558 amplifier, a 5.5-MHz-wide SAW filter (made by Andersen Laboratories), another UTO-558, and a Mini Circuits mixer. This second mixer, along with a 40.8-MHz crystal oscillator, will translate the signal to baseband (0 to 5.5 MHz). The signal will then pass through a video amplifier (a pair of AD5539 wideband op amps) and a TRW TDC1044 A/D converter. The samples from the converter will be the input of the 2-bit autocorrelator board. This will be the autocorrelator, or Zeeman, channel.

The 54-GHz phase-locking subsystem will center around an STS Instruments Model 800 lockbox. This device is designed to compare a mixed-down (to approximately 100 MHz) sample of the Gunn oscillator signal with a reference signal of the same frequency, so as to provide an error voltage for controlling the Gunn. The down-conversion is to be performed by an harmonic mixer and a phase-locked or synthesized signal source in the 2-GHz to 18-GHz range. The reference signal will be provided by an Analytic Instruments FS-125 62.5MHz-to-125MHz synthesizer module.

The autocorrelator board, which was essentially finished by June, 1989, still contained some errors in its interface to the host personal computer. Mike Petro, the board's designer, continued working with it and has eradicated all known problems.

Tests have been made to verify the performance of the radiometer front-end components. The basic function of the Electromagnetic Sciences ferrite calibration switch has been demonstrated. Tests of the Watkins-Johnson 54-GHz Gunn oscillator and mixer have not been so positive.

The manufacturer's test data for the oscillator/mixer combination indicate a worst-case noise figure of 3.9 dB across the oscillator's specified tuning range (52.8 GHz to 54.94 GHz). This noise figure was measured looking at the entire 10-MHz to 500-MHz IF passband of the mixer. We made measurements with a noise tube and a variable attenuator and with cryogenic and ambient loads. These measurements, while somewhat inconsistent, indicated a noise figure of about 8 dB measured across the entire IF passband. We have access to a Hewlett-Packard 8970A noise-figure meter and would like to use it to confirm these tests. We are trying to locate a compatible, calibrated V-band noise source.

The SAW-filter/2nd-mixer/crystal-oscillator module, the video-amplifier module, the A/D-converter module, and the FS-125 synthesizer are all to be assembled on printed circuit boards. The layout of these boards has begun.

2. SOUNDING THE STRATOPAUSE REGION FROM THE SURFACE

Upper-atmospheric emission from the strong oxygen lines cannot be observed from the surface because the lower atmosphere is opaque. However, on the wings of the oxygen band, the lower atmosphere is sufficiently transmissive to permit observation of lines arising from higher rotational levels (Waters, 1973). Figure 1 shows brightness temperatures near the 27- line, computed for the magnetic latitude of Boston. (The 1976 U.S. Standard Atmosphere was used in all of the computations here.) The linearly polarized component (the departure from circularity of the polarization ellipse) is a small fraction of a degree Kelvin in this case.

At any frequency, most of the brightness temperature is emitted from the lower atmosphere. Therefore, one takes the difference of two measurements, either at different frequencies or different polarizations, to measure the high-altitude emission. The vertical distribution of contributions to this brightness-temperature difference is a contribution function. Figure 2 plots the pressure level at which the contribution function peaks, as a function of the two frequencies of measurement.

To obtain a reasonable signal-to-noise ratio, one averages over a finite bandwidth, and thus one may generalize the differencing operation to

$$\Delta T_B(m,B) = \int_{m-B/2}^{m+B/2} K(\nu-m)\, T_B(\nu)\, d\nu, \qquad (1)$$

where $K(\nu)$ is an antisymmetric function of frequency ν, with total width B. Then ΔT_B is

related to the atmospheric temperature profile T(z) by

$$\Delta T_B(m,B) = \int_z \int_{m-B/2}^{m+B/2} K(\nu-m)\, W(\nu,z)\, d\nu\, T(z)\, dz$$

$$= A(m,B) \int_z C_N(m,B,z)\, T(z)\, dz, \qquad (2)$$

where $W(\nu,z)$ is the temperature weighting function at a frequency ν. A normalized contribution function $C_N(m,B,z)$, whose integral with respect to the vertical coordinate z is unity, is defined by the second line of Eq. 2. It is easily shown that the signal-to-noise ratio is maximized when

$$K(\nu) \propto \int_z [W(m+\nu,z) - W(m-\nu,z)]\, dz. \qquad (3)$$

One can choose the mean offset m and width B so that the frequency averaging does not excessively broaden the contribution function. As an example, for the line shown in Figure 1 in left-circular polarization, we take m = -0.5 MHz (with respect to line center) and B = 3.82 MHz. This corresponds to integration over the frequency range indicated by the dot-dash line in Figure 2. The function $K(\nu)$ is shown in Figure 3; for convenience, it is normalized so that

$$\int_0^{B/2} K(\nu)\, d\nu = 1. \qquad (4)$$

Figure 4 displays the resulting normalized contribution function C_N. It peaks at the 1 mbar level (~50 km altitude) which is typically near the stratopause. The dimensionless coefficient A(m,B) defined by Eq. 2 has the value A = 0.0221 for the $K(\nu)$ in Figure 3. A(m,B) contains a factor attributable to attenuation in the lower atmosphere. This attenuation (~6 dB) varies somewhat, depending on temperature and the amount of water vapor, but it can be estimated by measuring atmospheric emission with the wide-bandwidth channel of the 53-GHz radiometer.

The preceding analysis has not considered the dependence of line intensity on temperature. This effect is very significant for lines like 27-, which come from high rotational levels of the oxygen molecule. The opacity of the atmosphere at the levels of the contribution function (Figure 4) is small compared with unity. Under this condition, the temperature dependence of emitted integrated spectral intensity S is

$$S \propto \exp(T_R/T)/T, \qquad (5)$$

where T_R = 1566 K for the 27- line. Hence

$$TdS/SdT = T_R/T - 1 \approx 5.26, \quad (6)$$

at T ≈250 K. This means that a 1% increase in temperature over the region covered by the contribution function would increase the measured line intensity by 5.26%. Absorption and emission from the lower part of the atmosphere are contributed mostly by the wings of the stronger, lower rotational level oxygen lines, whose temperature dependence is much smaller.

The K(v) in Figure 3 has an effective bandwidth

$$B_{eff} = \left[\int_{-B/2}^{B/2} K^2(v)\, dv \right]^{-1} = 0.78 \text{ MHz}. \quad (9)$$

Therefore the antenna-temperature sensitivity is

$$\Delta T_{rms} = 1.15\,(T_N+T_A)\,(t\,B_{eff})^{-1/2} \approx 0.25 \text{ K}, \quad (10)$$

for integration t = 1 min., and T_N = 1300 K. The factor of 1.15 in Eq. 10 is the loss of signal-to-noise ratio in the digital correlator (Bos, 1986) that we plan to use. In a ground-based measurement, integration time is usually not a critical consideration, so the image sideband of the radiometer is placed in a featureless part of the spectrum. Hence the sensitivity to stratospheric line emission is reduced by a factor of two. Including this factor of two, the factor A from Eq. 2, and the increase in sensitivity due to temperature dependence (Eq. 6), the sensitivity to stratopause region temperature is 0.25K •2/(0.0221•5.26) = 4.3K in 1 min., or 1K in 20 min. observation of the 27- line.

REFERENCES

J.W. Waters, "Ground-based measurement of millimetre-wavelength emission by upper stratospheric O_2," *Nature* **242**, 506-508, 1973.

A. Bos, *The N.F.R.A. Correlator Chip*, Int. Tech. Rep. 176, Netherlands Found. for Radio Astron., Dwingeloo, 1986.

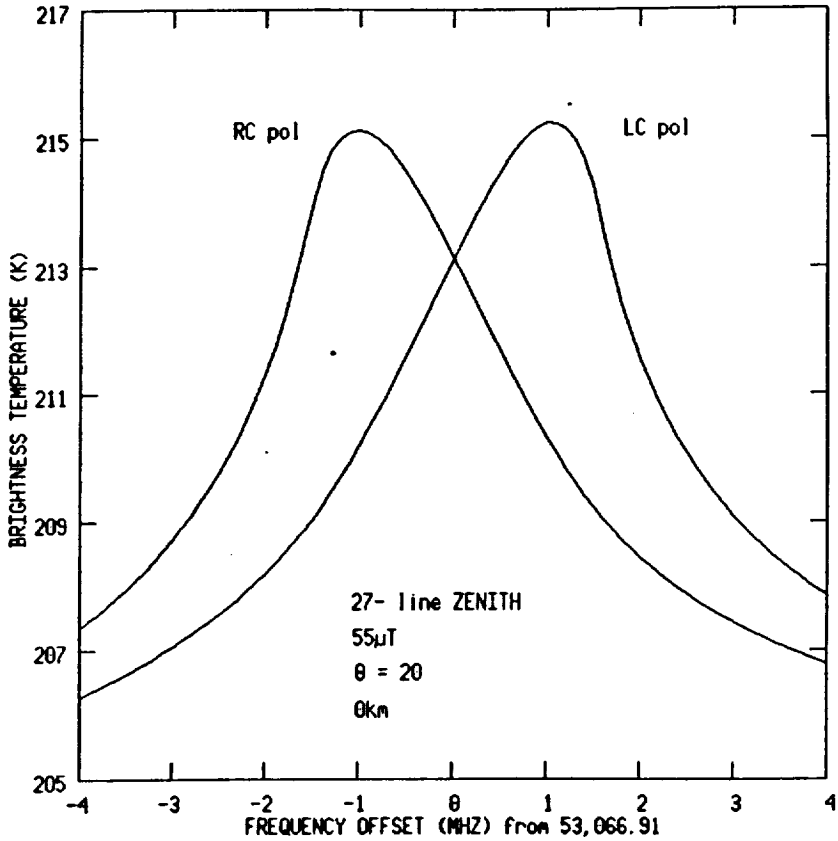

Fig. 1. Computed zenith brightness temperatures versus frequency near the 27- oxygen line.

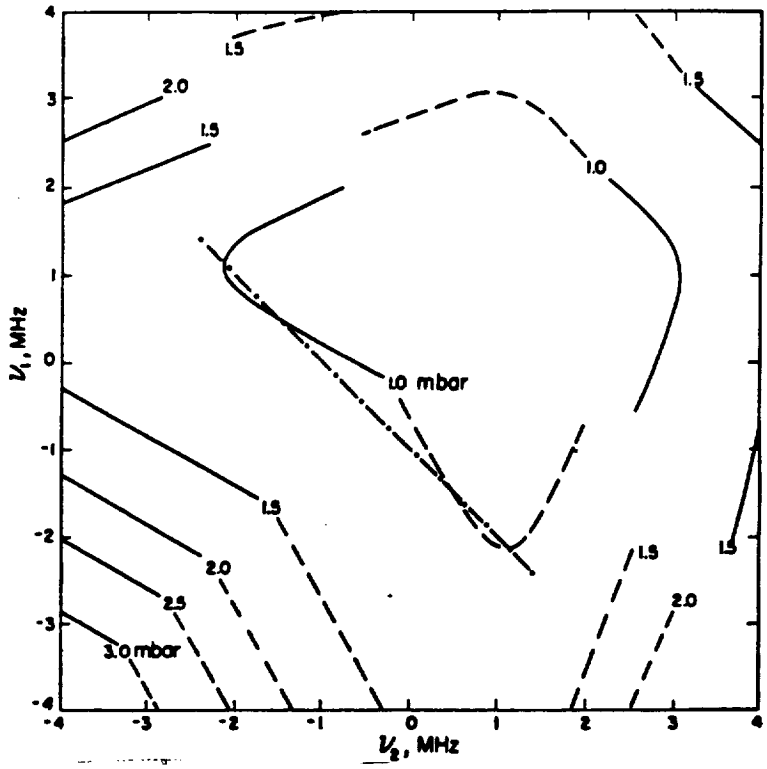

Fig. 2. Pressure level at the peak of the contribution function for $T_B(\nu_1)$-$T_B(\nu_2)$. Left-circular polarization was assumed, with the magnetic field as in Fig. 1. The dashed lines are drawn when the contribution function is negative. The dot-dash line is discussed in the text.

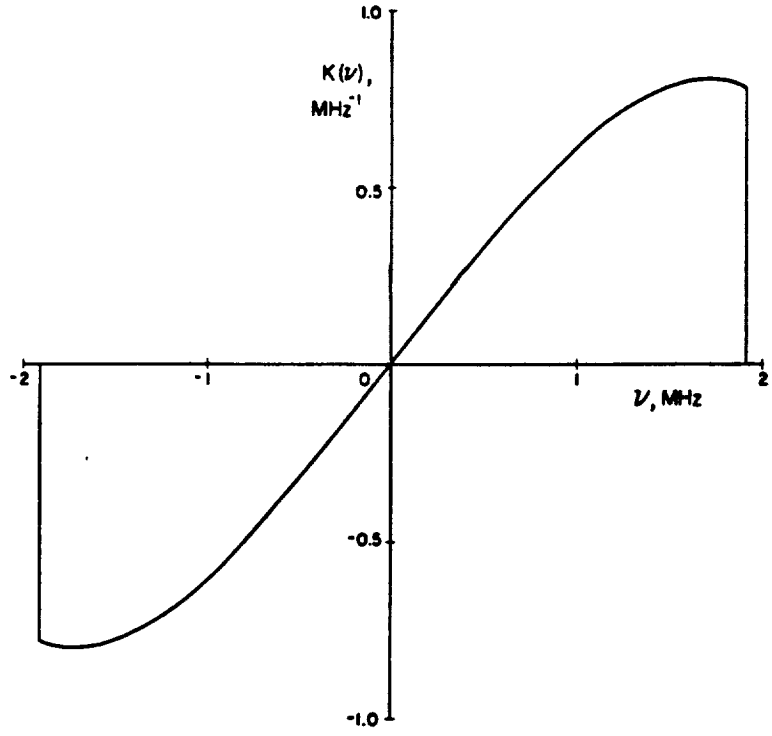

Fig. 3. Spectrum-weighting function.

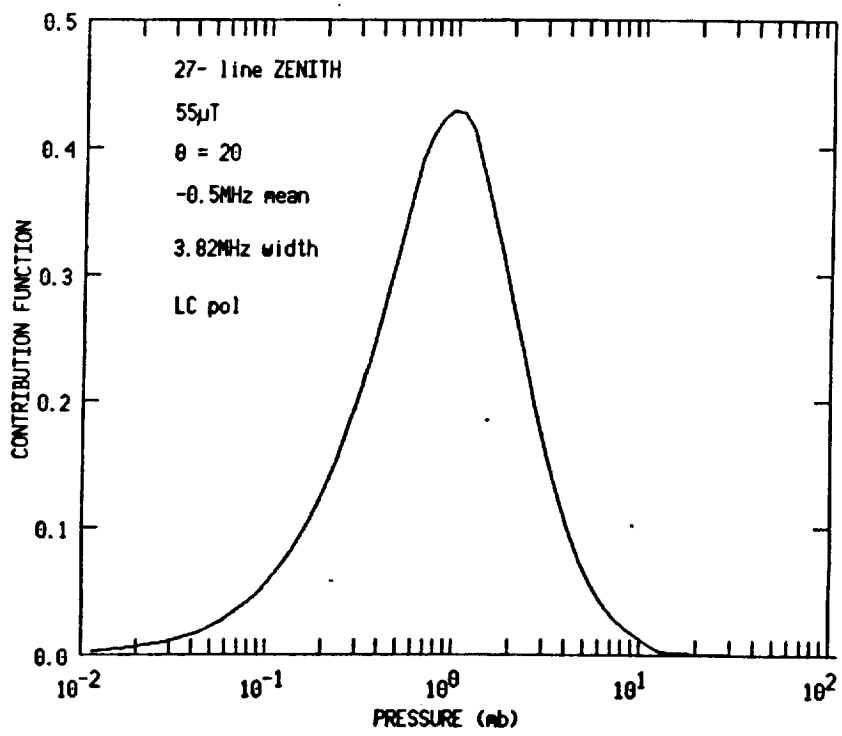

Fig. 4. Normalized contribution function for observation of the left-circularly polarized brightness temperature in Figure 1 with the spectrum-weighting function in Figure 3, centered at -0.5 MHz.

3. DETECTION AND MEASUREMENT OF RADIANCE WAVES IN 118-GHZ SPECTRAL IMAGES OF THE ATMOSPHERE

The object of this work is to develop sensitive new methods for detecting weak atmospheric waves in microwave radiometric data, and to use these methods to study the MTS 118-GHz and 54-GHz data obtained during the GALE, COHMEX, and FROZEN missions. As discussed in previous reports, the atmospheric wave detection and parameter estimation problems resemble those encountered in sonar and seismic data processing. The basic problem is one of estimating the power spectrum of a random space-time signal from received samples of that signal. The approach involves segmenting a frequency-wavenumber parameter space and then determining, for a particular location within that space, whether sufficient energy exists in the received signal to exceed a pre-determined decision threshold. Cases for which this criterion is met then become candidates for the application of parameter estimation algorithms specifically tailored to the atmospheric waves of interest.

Progress during this period consisted of work in the areas described below:

A. Amplitude Profile Estimation / Performance Analysis

A large fraction of the emphasis during the period was on the development of a mathematical formalism for use in determining the properties of observed wave events. The observable properties were found to consist of the frequency and wavenumber parameters yielded by the detection step and a specification of the magnitude and phase structure of the wave disturbance as a function of altitude.

Given knowledge of frequency and wavenumber, the amplitude profile estimation problem is a linear problem that permits a host of established techniques to be applied. However, because observed wave amplitudes are anticipated to lie below the noise threshold of the instrument, and because of the presence of a number of non-atmospheric interfering sources, the central issue in the analysis is achieving an estimator that has acceptable statistical properties and is robust to the class of disturbances present in this system.

The principal result of the analysis was the development of a maximum-likelihood (ML) based algorithm for estimating the continuous, complex-valued vertical amplitude profile of the wave. In conjunction with this work, an extensive analysis of the theoretical performance of the estimator was conducted in order to enable proper interpretation of the estimation results in the absence of independent ground truth. The analysis includes consideration of deterministic bias components introduced as a result of ambiguous frequency-wavenumber detection, as well as statistical errors deriving from the radiometric sensor noise. The estimator performance was found to depend most strongly on the wavelength of the disturbance, with small wavelengths permitting levels of retrieval error and resolution superior to those encountered in the static temperature profile retrieval problem (assuming, in both cases, the absence of a priori profile measurements).

B. Interference Discrimination

A second area of emphasis involved the development of techniques for discriminating between the radiometric signatures of atmospheric waves and the effects of non-geophysical interference sources. The techniques developed exploit subtle features that

distinguish the wave signature from a purely periodic signal. These include: (1) a distortion of the apparent wavefront of the wave, which arises as a result of the cylindrical scanning geometry employed by the instrument, (2) a characteristic attenuation of the observed signal with viewing angle, (3) variations in amplitude that correspond to those implied by the instrument channel weighting functions, and (4) variations in the relative direction of propagation, due to the flight path assumed by the instrument-bearing aircraft.

C. Data Surveying

The third phase of activity involved continued work in the application of various preliminary wave detection strategies to the large body of radiometric data gathered during the GALE and COHMEX meteorological experiments. The strategies applied consisted of a pre-filtering operation to isolate the small scale signal features, followed by various spectral estimation procedures. This effort proceeded in parallel with a visual survey of the video imagery recorded inflight, the results of which serve to further classify the data. The use of these preliminary strategies in conjunction with the interference discrimination techniques noted above resulted in no conclusive evidence of wave-induced temperature perturbations at signal levels comparable to the sensor noise level. However, further refinement of the detection algorithms is expected to reduce this detection threshold by up to an order of magnitude.

4. PUBLICATIONS

During this period two papers were published:

A. J. Gasiewski and D. H. Staelin, Numerical modeling of passive microwave O_2 observations over precipitation, *Radio Science, 25,* 3, pp 217-235, May-June 1990.

D. H. Staelin, Passive microwave sensing of the atmosphere from space, *Microwave Radiometry and Remote Sensing Applications,* P. Pampaloni, Ed., pp 151-167, 1989, VSP BV, Utrecht, The Netherlands.